Dalton Transactions

Accepted Manuscript

ROYAL SOCIETY OF CHEMISTRY

www.rsc.org/dalton

In situ synthesis of uniform Fe_2O_3/BiOCl p/n heterojunction and the improved photodegradation properties for mixture dyes

Na Li, Xia Hua, Kai Wang, Yujian Jin, Jingjing Xu, Mindong Chen and Fei Teng *

Jiangsu Engineering and Technology Research Center of Environmental Cleaning Materials (ECM), Jiangsu Key Laboratory of Atmospheric Environment Monitoring and Pollution Control (AEMPC), Jiangsu Joint Laboratory of Atmospheric Pollution Control (APC), Collaborative Innovation Center of Atmospheric Environment and Equipment Technology (AEET), School of Environmental Science and Engineering, Nanjing University of Information Science & Technology，219 Ningliu Road, Nanjing 210044, China. Email: tfwd@163.com (F. Teng); Phone/Fax: +86-25-58731090

Abstract

The *x*Fe_2O_3/*y*BiOCl composites (*x*Fe/yBi, *x/y* = 0/100, 5/100, 10/100, 20/100, 30/100, 40/100 molar ratios) are, for the first time, prepared through an in situ hydrolysis method under hydrothermal conditions. The samples are characterized by X-ray diffraction (XRD), scanning electron microscope (SEM), high-resolution transmission electron microscopy (HRTEM), selected area electron diffraction (SAED) and UV-vis diffused reflectance spectra (UV-DRS). The photodegradation performances of the *x*Fe/*y*Bi samples are mainly investigated using the mixture wastewater containing both rhodamine B (RhB) and methyl orange (MO) as the simulated industry wastewater. It is found that the uniform Fe_2O_3 nanocubes are well distributed on the BiOCl nanosheets. Moreover, the *x*Fe/*y*Bi photocatalysts exhibit the unexpectedly higher efficiencies than the bare BiOCl or Fe_2O_3

*Corresponding author. Email: tfwd@163.com (F. Teng); Phone/Fax: 0086-25-58731090

under ultraviolet light irradiation ($\lambda \leq 420$ nm). Specifically, the degradation rates of the *x*Fe/*y*Bi samples at *x/y* = 5/100 and 10/100 are 4 times higher than that of the bare BiOCl for MO-RhB mixture dyes. Their high photocatalytic activities are mainly attributed to the formation of stable p-n heterojunctions between the Fe_2O_3 and the BiOCl, which has greatly improved the separation of photogenerated carriers. Importantly, the highly efficient, inexpensive *x*Fe/*y*Bi p/n heterojunctions are expected to be applied in practical industry wastewater that containing complicated toxic components.

Keywords: In situ; Fe_2O_3/BiOCl; p/n heterojunction; mixture dyes

1. Introduction

Currently, environmental pollutions, such as water and soil, have caused increasing concerns than ever. Particularly for textile industry, the release of toxic organic dyes has become a serious environmental problem. [1,2] Due to highly stable chemical structures of synthetic dyes, they can not be degraded using conventional treatment methods, such as adsorption, chemical coagulation, extraction, membrane separation technology and so on. So the wastewaters released by textile industry can not meet more stringent international environmental standards. In recent years, photocatalysis technology has attracted much attention, since it is a potentially green technology to efficiently decompose organic dyes by utilizing solar energy. [3] However, it is still a big challenge to explore inexpensive, highly efficient photocatalysts, which can be applied in practices.

Recently, BiOCl, as an efficient, inexpensive photocatalyst, has been widely studied in the degradation of organic pollutants. [4-7] The layered structure of the BiOCl favors for the separation of the photo-generated electrons and holes, thus leading to a high activity. [8-10] However, the BiOCl can only absorb ultraviolet light because of its wide band gap (3.19–3.60 eV). So far, many efforts have been made to improve its photocatalytic activity by coupling with the other semiconductors, such as, BiOCl/Bi_2O_3, [11,12] PANI/BiOCl, [13] BiOI/BiOCl, [14] WO_3/BiOI, [15] $NaBiO_3$/BiOCl, [16] BiOCl/BiOBr, [17] Bi_2S_3/BiOCl, [18,19] Ag/AgCl/BiOCl, [20] Ag/AgX/BiOX, [21] BiOCl/Ag_3PO_4, [22] and so on. On the one hand, nevertheless, the BiOCl-based heterojunctions modified with BiOI, Ag, AgX and Ag_3PO_4, are expensive, which limits their practical applications. It is desirable to explore the low-cost materials to couple with the BiOCl. On the other hand, some of the preparation methods are cumbersome, for example, using toxic solvents [13] or expensive surfactant, [15,20,21] or finely

controlling pH values. [11,12,16,18] Therefore, a simple, economical and environmentally friendly method is highly needed to prepare BiOCl-based heterojunctions. In this study, the Fe_2O_3/BiOCl photocatalysts are prepared by a facile hydrothermal method. Herein, Fe_2O_3 is selected as a coupling component with the BiOCl on base of its following advantages: First, Fe_2O_3 is an abundant, low-cost and environmentally friendly chemical in nature, which is widely applied in magnetism, sensors and biologics and photocatalysis. [23-29] Secondly, its energy bands can well match those of the BiOCl, which favor for the transfers of photogenerated charges from one material to another. Thirdly, a stable heterojuction is easy to form between the n-typed Fe_2O_3 and the p-typed BiOCl semiconductors, which favors for the separation of photogenerated electrons and holes thus refrain effectively their recombination.

Furthermore, more than one kind of pollutants (e.g., different organic compounds, heavy metal ions, alkaline or acidic substances, etc.) is generally contained in practical industrial wastewaters. To the best of our knowledge, however, most of researches are mainly focused on the degradation of single pollutant, fewer have report the degradation performances of the photocatalysts under the co-presence of multi-component pollutants. It is needed to develop an efficient and inexpensive photocatalyst that can effectively degrade industrial wastewaters containing multiple organic dyes.

Herein, the uniform Fe_2O_3/BiOCl p/n heterojunctions are, for the first time, prepared by a simple in situ hydrolysis method. We have investigated the activities of the catalysts at different molar ratios of the Fe_2O_3 to BiOCl. Furthermore, our main attention is paid to their photodegradation performances for the simulated the RhB-MO mixture wastewater. Here RhB is considered to be a cationic dye while MO is an anionic dye. The influences of different dye degradation have been briefly discussed. This contribution is aimed to extend photocatalysis technology to the practical applications.

2. Experimental

2.1. Materials and preparation

All chemicals were of analytical regent grade (A.R.), and used without further purification. Bismuth nitrate pentahydrate ($Bi(NO_3)_3 \cdot 5H_2O$), sodium chloride (NaCl) and ethylene glycol (EG) were purchased from the Sinopharm Chemical Reagent Co., Ltd. Iron chloride hexahydrate ($FeCl_3 \cdot 6H_2O$) was purchased from Guangzhou Jinhuada Chemical Reagent Co., Ltd.

Preparation of xFe/yBi samples. A simple, in situ hydrolysis method under hydrothermal conditions was used to synthesize the *x*Fe/*y*Bi samples. The BiOCl sample was prepared by a simple solvothermal synthesis method, which was described in electronic supporting information (ESI). Typically, 0.4 mmol of the $FeCl_3 \cdot 6H_2O$ was added into 50 mL of distilled water. After the $FeCl_3 \cdot 6H_2O$ was dissolved fully, 1 mmol of the as-prepared BiOCl powder was then added to the solution and stirred for 30-min by a magnetic stirrer. After that, the mixture was transferred into a Teflon-lined stainless steel autoclave and maintained at 160 °C for 12 h. The as-obtained sample was then washed with distilled water for several times and dried at 60 °C for 5 h. In order to achieve the optimum photocatalysts，the nominal molar ratio of the Fe_2O_3 to BiOCl varies from 5/100, 10/100, 20/100, 30/100 to 40/100 in our experiment (the real ratio of Fe/Bi are present in electronic supporting information (Table S1)). Furthermore, the phase-pure Fe_2O_3 sample was also prepared under the same conditions without adding the BiOCl. Herein, the as-prepared pure Fe_2O_3, $x Fe_2O_3/y$BiOCl and the phase-pure BiOCl samples were labeled as 0Fe/100Bi, 5Fe/100Bi, 10Fe/100Bi, 20Fe/100Bi, 30Fe/100Bi, 40Fe/100Bi and 100Fe/0Bi, respectively.

2.2. Photocatalytic degradation reactions

Photocatalytic activities of the samples were evaluated by photocatalytic decomposition of rhodamine B (RhB), methyl orange (MO), methylene blue (MB) and the RhB-MO mixture wastewater, respectively. Typically, 0.05 g of powder was respectively added into the solution (200 mL, 10 mg/L), which was irradiated with a 300 W Xe arc lamp equipped with ultraviolet light ($\lambda \leq 420$ nm). The suspension was stirred for 30 min to reach an adsorption–desorption equilibrium of dye molecules on the surface of photocatalyst. During photoreaction, 4 mL of suspension was collected at a given interval time and centrifuged to remove the particles. The concentration of dye remained in the solution was determined by using UV–vis spectrophotometer. For the RhB-MO mixture wastewater, 200 mL of 10 mg/L RhB and 10 mg/L MO are employed.

2.3. Characterization

The crystal structures of the samples were determined by X-ray powder polycrystalline diffractometer (Rigaku D/max-2550VB), using graphite monochromatized CuK_α radiation (λ= 0.154 nm), operating at 40 kV and 50 mA. The XRD patterns were scanned in the range of 20-80^o (2θ) at a scanning rate of 5^o min^{-1}. The samples were characterized on a scanning electron microscope (SEM, Hitachi SU-1510) with an acceleration voltage of 15 keV. The samples were coated with 5-nm-thick gold layer before observations. The fine surface structures of the samples were determined by high-resolution transmission electron microscopy (HRTEM, JEOL JEM-2100F) equipped with an electron diffraction (ED) attachment with an acceleration voltage of 200 kV. The texture properties of the samples were measured by nitrogen sorption isotherms. The surface areas and pore size distribution of the samples were calculated by the Brunauer-Emmett-Teller (BET) and Barret-Joyner-Halender (BJH) methods, respectively. UV-vis diffused reflectance spectra

(UV-DRS) of the samples were obtained using a UV-vis spectrophotometer (UV-2550, Shimadzu, Japan).

3. Results and discussion

3.1. Characterization of *x*Fe/*y*Bi samples

Fig. 1(a,b) shows the representative SEM image of the typical BiOCl sample. The as-prepared sample is composed of microspheres, whose diameters range from 4 to 7 μm. Moreover, these microspheres are well separated one another, although they have discrepant diameters. It is interesting that the microspheres are assembled by numerous nanosheets, in which many pores can form. Such porous structure favors for the adsorption and desorption of dyes; as well for the multiple reflections and absorptions of irradiated light, which can take full advantage of irradiation light (Fig. 2). So the nanosheet-assembled microsphere structure plays an important role in the photocatalytic reaction. Fig. 1c shows the XRD patterns of the sample. All the diffraction peaks of the sample are in good agreement with those of the standard BiOCl (JCPDS 06–0249), indicating the phase-pure BiOCl is obtained. After being coupled with the Fe_2O_3, some of microspheres have broken into pieces, the others microspheres have become loose, as shown in Fig. 1d. It was found that before hydrothermal reaction, the pH values of the $FeCl_3$ solutions were 2.16~2.57 at different amounts added. After hydrothermal reaction, the pH values have decreased to 1.7~2.46 due to the hydrolysis of Fe (III) ions. It is a fact that the hydrogen ions generated in the system will increase. As the BiOCl itself can dissolve in acidic solution, it is reasonable that the edges of nanosheets can dissolve in acidic solution. As a result, the microspheres can gradually become loose, even broke into pieces, as shown in Fig. 1d. In Fig. 1c, the diffraction peaks of the Fe_2O_3 can not be observed for 10Fe/100Bi sample, which may be due to some diffraction peaks of Fe_2O_3 overlap with those of the BiOCl (e. g., the diffraction peaks at 33.5° and 54°).

Moreover, the small size and small amount of Fe_2O_3 (Table S1 of ESI) on the BiOCl nanosheets also result in the decreasing of peaks intensities. Besides, Table 1 presents the texture properties of the *x*Fe/*y*Bi samples. The surface areas of the *x*Fe/*y*Bi samples are almost identical (about 1 m^2/g), indicating that the amount of the Fe_2O_3 added has little influence on the texture properties of the coupled samples. In contrast, the surface area of the pure BiOCl is 15 m^2/g, which is significantly higher than those of *x*Fe/*y*Bi samples. Also, the pore volumes of the *x*Fe/*y*Bi samples are smaller than that of the pure BiOCl. The decrease of surface areas and pore volumes of the *x*Fe/*y*Bi samples may be due to the microstructure change from the porous BiOCl microspheres to the *x*Fe/*y*Bi nanosheets. Fig. 3 shows the XRD patterns of the samples. It is observed that compared with BiOCl, all the diffraction peak positions of the BiOCl in the *x*Fe/*y*Bi samples have not shifted, indicating that Fe (III) ions have not inserted into the lattice or substituted for Bi (III) ions of the BiOCl. At higher *x/y* values than 10/100 (molar ratios), besides the diffraction peaks of the BiOCl, the diffraction peaks of the Fe_2O_3 are observed. Moreover, the (110) peak intensity of the Fe_2O_3 increases gradually with increasing the amount of the Fe_2O_3 added.

Furthermore, Fig. 4 displays the high-resolution electron emission microscopy (HRTEM) images and selected area electron diffraction (SAED) pattern of the 10Fe/100Bi sample. It is clearly observed from Fig. 4(a,b) that the cubic Fe_2O_3 nanoparticles uniformly distribute on the BiOCl nanosheets through the dark-bright contrast resulting from the different atomic densities of the Fe_2O_3 and the BiOCl. It is clear that the sides lengths of the Fe_2O_3 cubes are about 30~50 nm. Fig. 4c shows SAED pattern of the sample. The clear diffraction spots result from the (200) and (110) Bragg reflections of the BiOCl and the (110) Bragg reflections of the Fe_2O_3, respectively. Moreover, the interface between the Fe_2O_3 and the BiOCl is observed by HRTEM (Fig. 4d). The lattice spacing of 0.248 nm is well indexed to the (110) crystal plane of the Fe_2O_3, while that of 0.273 nm matches the (110) crystal plane of the BiOCl. The

HRTEM results firmly confirm the formation of *x*Fe/*y*Bi heterojunctions.

3.2. Photocatalytic activities of the samples

3.2.1. Photocatalytic activities for single-component wastewater

Our measurement results show (Fig. S1 of ESI) that under visible light irradiation, the *x*Fe/yBi heterojunctions almost have no catalytic activity, which may be closely relative to the visible light responsive Fe_2O_3. It has been reported [27,30,31] that due to the short diffusion length of photogenerated holes in the Fe_2O_3, the photogenerated electron–hole pairs can not be separated easily, because they are easy to recombine again. Thus, all the photocatalytic activities of the samples were evaluated under ultraviolet light irradiation. It is clearly observed from Fig. 5(a,b) that the photocatalytic degradation efficiencies of RhB over these samples follow the order: 10Fe/100Bi > 5Fe/100Bi > 20Fe/100Bi > 30Fe/100Bi > 40Fe/100Bi > 0Fe/100Bi > 100Fe/0Bi. The *x*Fe/*y*Bi heterojunctions have the improved photocatalytic activities. In particular, the 10Fe/100Bi sample exhibits the highest photocatalytic activity for the degradation of RhB among the samples, and 98% of RhB has been degraded after 20-min UV light irradiation. In contrast, only 88% of RhB can be degraded after 40-min irradiation for the pure BiOCl. It is obvious that the optimum molar ratio of the Fe_2O_3 to the BiOCl is 10/100 for the photocatalytic degradation of RhB. With further increasing the amount of Fe_2O_3, the photocatalytic activity of the *x*Fe/*y*Bi photocatalyst decreases. It may be that at a too high x/y ratio, more Fe_2O_3 nanoparticles have agglomerated and even separated from the surface of BiOCl (Fig. S2d). Furthermore, it has been reported [27,30,31] that the photogenerated electron–hole pairs of Fe_2O_3 are easy to

recombine again. So the photocatalytic degradation efficiencies of the *x*Fe/*y*Bi samples decrease at too higher Fe_2O_3 amounts. Besides, the pure BiOCl has a higher photocatalytic activity than the pure Fe_2O_3. It is well known [27,30,31] that the Fe_2O_3 has a short diffusion length of photogenerated holes, resulting in a higher recombination rate of photogenerated electrons and holes, compared with the BiOCl that has a layered structure favoring for the separation of photogenerated carriers. [8-10] Further, we have investigated the photodegradation of mehylene orange (MO, an anionic dye). As shown in Fig. 5(c,d), the *x*Fe/*y*Bi heterojunctions also show the improved photocatalytic activity for the degradation of MO, compared with the pure BiOCl. Moreover, the optimum molar ratio of the Fe_2O_3 to the BiOCl is 5/100.

The photodegradation of RhB or MO can be simplified as the pseudo-first-order kinetic reaction, as described as the following formulae.

$$\ln(C_0/C) = k_a \times t, \quad (1)$$

Where C is the concentration of RhB or MO remained in the solution after irradiation and C_0 is the initial concentration of RhB or MO before irradiation. Fig. 5b and 5d present the plots of $\ln(C_0/C)$ versus irradiation time for the degradations of RhB and MO, respectively. The *x*Fe/*y*Bi heterojunctions have the notably high reaction rates in a wide x/y molar range, whereas the pure BiOCl or Fe_2O_3 has a low reaction rate. The calculated apparent rate constants (k_a) for the degradations of RhB and MO are given in Table 2, respectively. It is obvious that for the decomposition of RhB, 10Fe/100Bi sample has the highest reaction rate among the samples and the k_a value of the 10Fe/100B is 4 and 16 times higher than those of the pure BiOCl and Fe_2O_3, respectively. For the degradation of MO, the k_a value of the 5Fe/100Bi sample is the largest among them, which is about 7 and 19 times higher than those of the pure Fe_2O_3 and BiOCl, respectively. At same time, the *x*Fe/yBi composites also show

the improved photocatalytic activities than pure BiOCl and Fe_2O_3 for the degradation of methylene blue (Fig. S3 of ESI). It is worth noting that the *x*Fe/*y*Bi heterojunctions can mineralize dyes because the reports [9,10,14] have demonstrated this using TOC or LC–MS method.

3.2.2. Photocatalytic activities for RhB-MO mixture wastewater

Generally, more than one dye is contained in practical wastewater. In order to simulate practical wastewater, the photoderadation of the RhB-MO mixture dye solution was employed to investigate the degradation activities of the samples under ultraviolet light irradiation. It is found that the positions of maximum absorption peaks for RhB and MO dyes have not changed in the mixture dye solution, as shown in Fig. 6. The absorbencies of RhB and MO in mixture wastewater were still measured at 552 nm and 463 nm, respectively. Fig. 7 shows the photocatalytic activities of the samples for the RhB-MO mixture dye solution. Compared with the pure BiOCl, *x*Fe/*y*Bi heterojunctions show the improved photocatalytic activities under ultraviolet light irradiation. The 5Fe/100Bi photocatalyst show the highest activity for the RhB-MO mixture solution. After 30-min ultraviolet light irradiation, more than 90% of RhB (Fig. 7a) and 90% of MO (Fig. 7c) in the RhB-MO mixture dye solution are degraded by the 5Fe/100Bi photocatalyst. We also prepared the composites of 0.05 mmol Fe_2O_3 and 1 mmol BiOCl by mechanical grinding method, and test its degradation activity. It is obvious that its photocatalytic activity is almost same as that of BiOCl, but is far lower than that of the 5Fe/100Bi heterojunction. The photodegradation reaction of the RhB-MO mixture dyes can also be simplified as the pseudo-first-order kinetics reaction. Fig. 7b and 7d present the kinetic curves of RhB and MO in mixture dyes solution, respectively. Their apparent reaction rate constants (k_a) are given in Table 2. The 5Fe/100Bi sample has a k_a value much larger than the others samples for the degradation of the RhB-MO mixture dyes solution. Besides, it is also

observed that the degradation rate of MO is faster than that of the RhB dye (Table 2 and Table S2 of ESI). The apparent rate constant of MO is about 2 times as high as that of RhB over the 5Fe/100Bi photocatalyst.

Fig. S4 (seeing ESI) shows the adsorption amounts of RhB and MO dyes over the 5Fe/100Bi sample in the RhB-MO mixed solution under dark condition. The average adsorption amount of the RhB over the sample is 7.8%, but that of MO is 1.8%. It is obvious that over the 5Fe/100Bi sample, the adsorption amount of the RhB is 4 times as large as that of the MO; however, the degradation rate of MO is 2 times as high as that of the RhB over the same 5Fe/100Bi catalyst, indicating that a larger adsorption amount does not always mean a high degradation activity. Herein we hold that their different degradation rates are mainly associated with their different molecule structures, as shown in Fig. S5 (seeing ESI). Rauf et al. have reported that azo bonds (–N=N–) are the most active in azo dye molecules and can be easily oxidized by hydroxyl radicals or positive holes. [32] But the RhB dye has a stable chemical structure. As a result, the degradation rate of MO is higher than that of the RhB. Furthermore, it should be noted that in the single dye solution, the degradation rates of the RhB and MO are 3.4-6.7 and 1.4-3.8 times as high as those in mixture dye solution over the same sample, respectively (Table 2). It is obvious that there is a strong interaction among the components in mixture dye solution. We hold that in the co-presence of both the RhB and MO, the activity decrease may mainly result from their competitive adsorptions. Both the RhB and MO can adsorb on the surfaces of the catalysts simultaneously. As a result, the degradation rate of the RhB-MO mixture solution is slower than that of single-dye. To conclude, the *x*Fe/*y*Bi photocatalyst is promising to be applied in cleaning industry wastewater that generally contains more than one dye. Future work will mainly focus on the degradation performance of the *x*Fe/*y*Bi for more complicate wastewaters containing heavy metals ions, acids or alkalines, and other organic pollutants, so as to extend photocatalysis technology to practical wastewaters.

3.3. Formation of *x*Fe/*y*Bi heterojunctions and photocatalytic mechanism

It is well-known that the activity of photocatalyst is strongly dependent on the generation and separation of photogenerated charges. [33,34] The transfer rate and the separation efficiency of interfacial charges can be effectively improved by the coupled *x*Fe/*y*Bi samples with the matched conduction band (CB) and valence band (VB), as schematically illustrated in Fig. 8. The CB (-1.1eV) of BiOCl lies above the CB (0.28 eV) of Fe_2O_3, and the VB (2.48 eV) of Fe_2O_3 lies below that (2.4eV) of the BiOCl. Both the BiOCl and the Fe_2O_3 have the matched energy bands. Thus, a stable heterojuction is easy to form between the n-typed Fe_2O_3 and the p-typed BiOCl semiconductors. [35,36] Consequently, an internal electric field is built in the *x*Fe/*y*Bi heterojunction interface. Under UV light irradiation, both the Fe_2O_3 and BiOCl can be excited. Driven by the internal electric field, the photogenerated electrons at the CB of the BiOCl can migrate to the CB of the Fe_2O_3. Simultaneously, the generated holes in the VB of the Fe_2O_3 can move along the opposite direction to that of the BiOCl. As a result, the recombination rate of the photogenerated electrons and holes can be reduced effectively, and the photocatalytic activity of the *x*Fe/*y*Bi photocatalyst can be improved greatly, compared with the pure BiOCl or Fe_2O_3. Moreover, the UV–DRS spectra show that the light absorption ability of the *x*Fe/yBi samples also have been improved than BiOCl or Fe_2O_3 (Fig. S6 of ESI), which also favors for the improvement of photocatalytic activity.

4. Conclusions

The Fe_2O_3/BiOCl p/n heterojunctions can be easily synthesized by an in situ hydrolysis method. Compared with BiOCl or Fe_2O_3, the Fe_2O_3/BiOCl heterojunctions exhibit fairly higher activities not only for individual RhB or MO dye but also for the RhB-MO mixture dyes. Their high degradation activities are mainly attributed to the formation of a stable p-n heterojunction between Fe_2O_3 and BiOCl, which has refrained greatly the recombination of

photogenerated carriers. Future work will mainly focus on the degradation performance of *x*Fe/*y*Bi for more complicate toxic wastewaters containing heavy metals ions, acids or alkalines, and other organic pollutants, so as to extend photocatalysis technology to practical wastewaters.

Acknowledgements

This work is financially supported by National Science Foundation of China (21377060, 21103049), the Key Project of Environmental Protection Program of Jiangsu (2013016, 2012028), the Project Funded by the Science and Technology Infrastructure Program of Jiangsu (BM201380277, 2013139), Jiangsu Science Foundation of China (BK2012862), Six Talent Climax Foundation of Jiangsu (20100292), Jiangsu Province of Academic Scientific Research Industrialization Projects (JHB2012-10, JH10-17), A Project Funded by the Priority Academic Program Development of Jiangsu Higher Education Institutions (PAPD) sponsored by SRF for ROCS, SEM (2013S002) and "333" Outstanding Youth Scientist Foundation of Jiangsu (2011015).

References

[1] M. Gonçalves, M.C. Guerreiro, L.C.A.D. Oliveira and C.S.D. Castro, J. Environ. Manag. 2013, 127, 206−211.

[2] L.L. Yuan, D.D. Huang, W.N. Guo, Q.X. Yang and J. Yu, Appl. Clay Sci. 2011, 53, 272−278.

[3] M.R. Linford, M. Auch and H. Mohwald, J. Am. Chem. Soc. 1998, 120, 178−182.

[4] J.M. Ma, X.D. Liu, J.B. Lian, X.C. Duan and W.J. Zheng, Cryst. Growth & Des. 2010, 10, 2522−2527.

[5] K. Li, Y.L. Xu, Y. He, C. Yang, Y.L. Wang and J.P. Jia, Environ. Sci. & Technol. 2013, 47, 3490−3497.

[6] H.L. Peng, C.K. Chan, S. Meister, X.F. Zhang and Y. Cui, Chem. Mater. 2009, 21, 247−252.

[7] K. Zhang, J. Liang, S. Wang, J. Liu, K.X. Ren, X. Zheng, H. Luo, Y.J. Peng, X. Zou, X. Bo, J. Li and X.B. Yu, Cryst. Growth & Des. 2012, 12, 793−803.

[8] J. Jiang, K. Hao, X.Y. Xiao and L.Z. Zhang, J. Am. Chem. Soc. 2012, 134, 4473–4476.

[9] X. Xiao, R. Hao, M. Liang, J. Hazard. Mater. 2012, 233, 122-130.

[10] B. Pare , B. Sarwan, S.B. Jonnalagadda, Appl. Surf. Sci. 2011,258, 247– 253.

[11] A.K. Chakraborty, S.B. Rawal, S.Y Han, S.Y. Chai and W.I. Lee, Appl. Catal. A: Gen. 2011, 407, 217–223.

[12] S.Y. Chai, Y.J. Kim, M.H. Jung, A.K. Chakraborty, D. Jung and W.I. Lee, J. Catal. 2009, 262, 144–149.

[13] Q.Z. Wang, J. Hui, J.J Li, Y.X. Cai, S.Q. Yin, F.P. Wang and B.T. Su, Appl. Surf. Sci. 2013, 283, 577–583.

[14] T.B. Li, G. Chen, C. Zhou, Z.Y. Shen, R.C. Jin and J.X. Sun, Dalton T. 2011, 40, 6751–6758.

[15] S. Shamaila, A.K.L. Sajjad, F. Chen and J.L. Zhang, J. Colloid Interface Sci. 2011, 356, 465–472.

[16] X.F. Chang, G. Yu, J. Huang, Z. Li, S.F. Zhu, P.F. Yu, C. Cheng, S.B. Deng and G.B. Ji, Catal. Today 2010, 153, 193–199.

[17] J. Zhang, J.X. Xia, S. Yin, H.M. Li, H. Xu, M.Q. He, L.Y. Huang and Q. Zhang, Colloids Surf. A 2013, 420, 89–95.

[18] J. Cao, B.Y. Xu, H.L. Lin, B.D. Luo and S.F. Chen, Catal. Commun. 2012, 26, 204–208.

[19] H.F. Cheng, B.B. Huang, X.Y. Qin, X.Y. Zhang and Y. Dai, Chem. Commun. 2012, 48, 97–99.

[20] W. Xiong, Q.D. Zhao, X.Y. Li and D.K. Zhang, Catal. Commun. 2011, 16, 229–233.

[21] L.Q. Ye, J.Y Liu, C.Q. Gong, L.H. Tian, T.Y. Peng and L. Zan, ACS Catal. 2012, 2, 1677−1683.

[22] B.C. Cao, P.Y. Dong, S.Cao and Y.H. Wang, J. Am. Ceram. Soc. 2013, 96, 544–548.

[23] X.L. Cheng, J.S. Jiang, M. Hu, G.Y. Mao, F.X. Bu, C.C. Lin, Y. Zeng and Q.H. Zhang CrystEngComm 2012, 14, 7701–7708.

[24] C.X. Xia, Y. Jia, M. Tao and Q.M. Zhang, Phys. Lett. A 2013, 377, 1943–1947.

[25] B. Palanisamy, C.M. Babu, B. Sundaravel, S. Anandan and V. Murugesan, J. Hazard. Mater. 2013, 252–253, 233–242.

[26] C.Q. Zhu, Y.R. Li, Q. Su, B.B. Lu, J.Q. Pan, J.W. Zhang, E.Q. Xie and W. Lan, J. Alloys Compd. 2013, 575, 333–338.

[27] S.W. Zhang, W.Q. Xu, M.Y. Zeng, J.X. Li, J.Z. Xu and X.K. Wang, Dalton T. 2013, 42, 13417–13424.

[28] Y. Zhang, Y.R. Zhang and J. Tan, J. Alloys Compd. 2013, 574, 383–390.

[29] W. Xiao, Z.X. Wang, H.J. Guo, Y.H. Zhang, Q. Zhang and L. Gan, J. Alloys Compd. 2013, 560, 208–214.

[30] S. Li, G.W. Qin, X.Y. Meng, Y.P. Ren and L. Zuo, J. Mater. Sci. 2013, 48, 5744–5749.

[31] A. Kay, I. Cesar and M. Grätzel, J. Am. Chem. Soc. 2006, 128, 15714–15721.

[32] M.A. Rauf, M.A. Meetani and S. Hisaindee, Desalination 2011, 276, 13–27.

[33] Y. Ren, M. Chen, Y. Zhang and L.M. Wu, Langmuir 2010, 26, 11391–11396.

[34] C.S. Pan, J. Xu, Y.J. Wang, D. Li and Y.F. Zhu, Adv. Func. Mater. 2012, 22, 1518–1524.

[35] Y.H. Hong, H.Y. Guai, S. Liu, R.Y. Jiang, Ceram. Int. 2014, 40, 9095–9100.

[36] J. Cao, C.C. Zhou, H.L. Lin, B.Y. Yan, S.F. Chen, Appl. Surf. Sci. 2013, 284, 263–269.

Title list of Tables and Figures

degradation of RhB-MO mixture solution (200 mL, 10 mg/L RhB + 10 mg/L MO) under UV irradiation ($\lambda \leq 420$ nm): (a,b) RhB; (c,d) MO; A: 0Fe/100Bi; B: 5Fe/100Bi; C: 10Fe/100Bi; D: 20Fe/100Bi; E: 30Fe/100Bi; F: 0Fe/100Bi; G: 100Fe/0Bi; H: the simple mixture of 0.05 mmol Fe_2O_3 and 1 mmol BiOCl

Fig. 8. Schematic diagram of photogenerated carriers transportation over the *x*Fe/*y*Bi heterojuctions

Table 1

Table 1 Texture properties of the *x*Fe/*y*Bi samples (*x/y*, the molar ratio of Fe_2O_3 to BiOCl)

Sample	[a] BET surface area (m^2/g)	[b] Pore volume (cm^3/g)	[b] Pore Diameter (nm)
0Fe/100Bi	15.9	0.056	10.7
5Fe/100Bi	1.6	0.009	36.8
10Fe/100Bi	1.8	0.009	35.7
20Fe/100Bi	1.7	0.015	34.3
30Fe/100Bi	1.1	0.012	39.5
40Fe/100Bi	2.1	0.023	40.7

Notes: [a], calculated by the Brunauer-Emmett-Teller (BET) method; [b], calculated by the Barret-Joyner-Halender (BJH) method

Table 2

Table 2 Apparent reaction rate constants (k_a) of the RhB, MO and RhB-MO mixture wastewater over *x*Fe/*y*Bi samples after 20 min UV irradiation ($\lambda \leq 420$ nm)

*x*Fe/*y*Bi samples	k_a (Single-component RhB solution) (min^{-1})	k_a (RhB in mixture solution) (min^{-1})	k_a (Single-component MO solution) (min^{-1})	k_a (MO in mixture solution) (min^{-1})
0Fe/100Bi	0.03861	0.00831	0.02516	0.01809
5Fe/100Bi	0.14412	0.04178	0.18149	0.09314
10Fe/100Bi	0.16621	0.03198	0.12365	0.08457
20Fe/100Bi	0.07662	0.01144	0.05118	0.02392
30Fe/100Bi	0.05937	0.01125	0.05684	0.03495
40Fe/100Bi	0.04208	0.00799	0.04612	0.03074
100Fe/0Bi	0.01011	0.00171	0.00955	0.00251

RhB, 200 mL, 10 mg/L; MO, 200 mL, 10 mg/L; RhB-MO, 200 mL of 10 mg/L RhB + 10 mg/L MO

Fig. 1

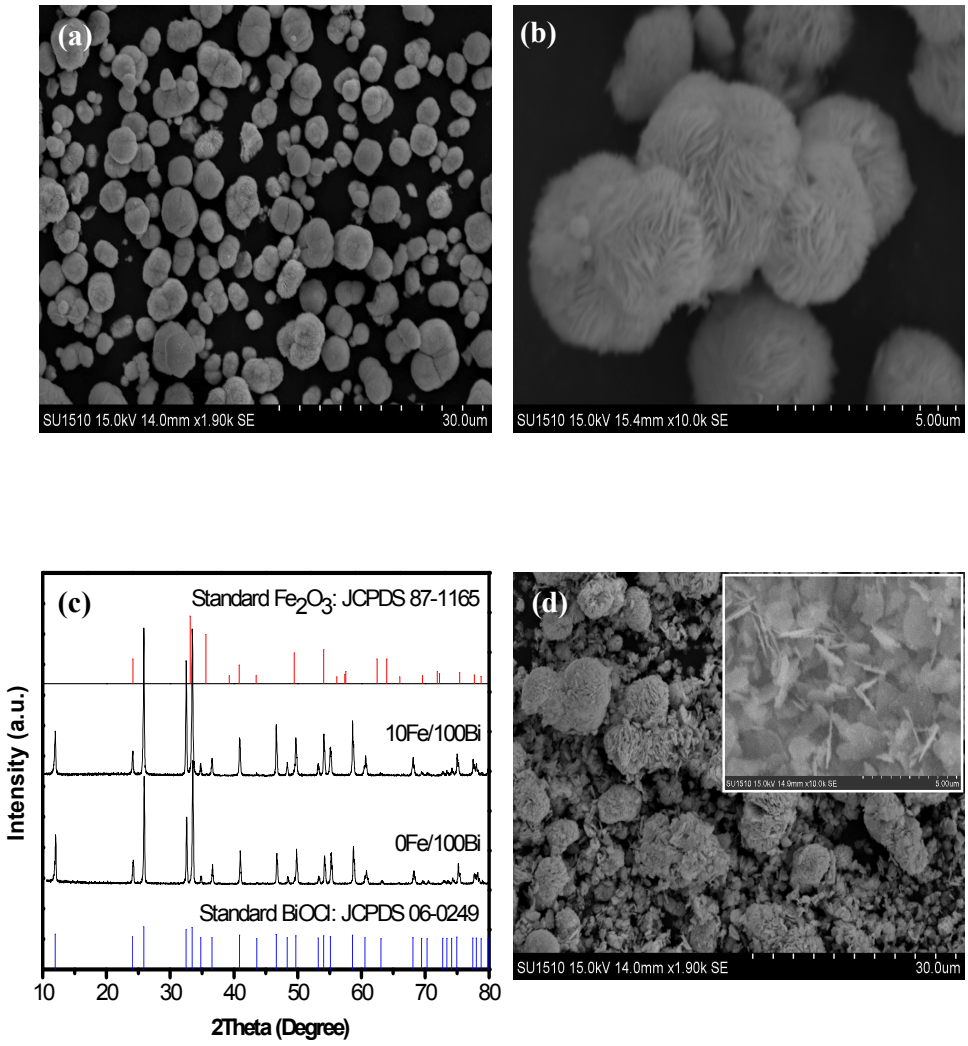

Fig. 2

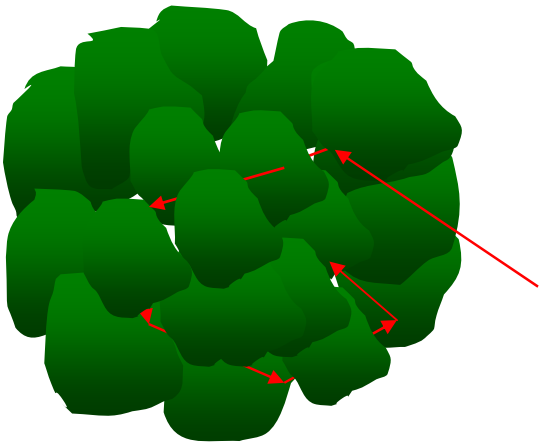

Fig. 3

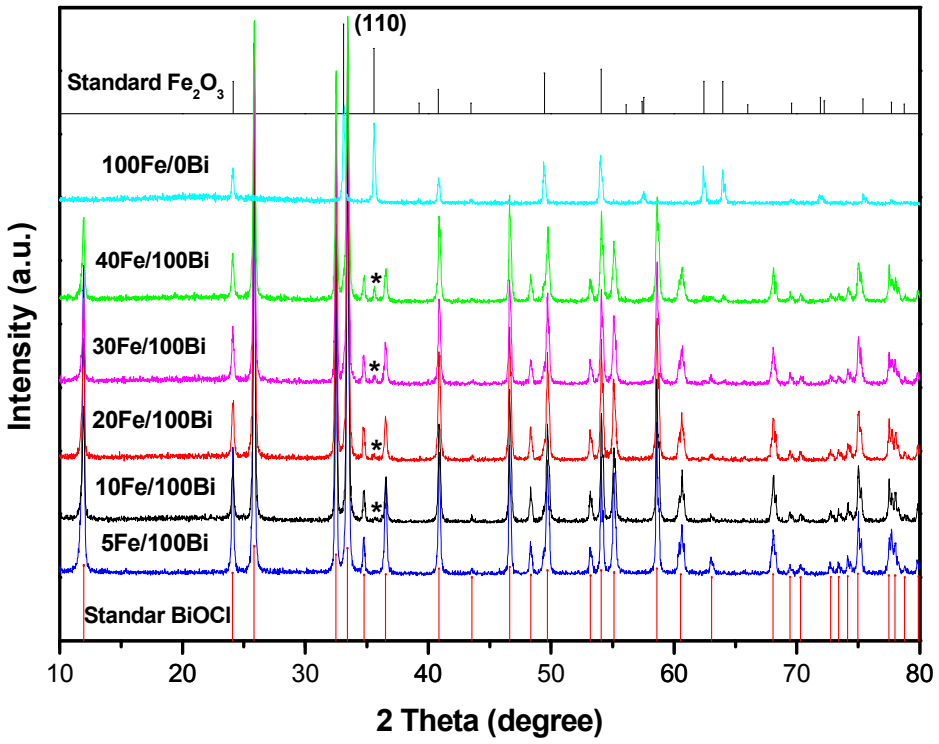

Fig. 4

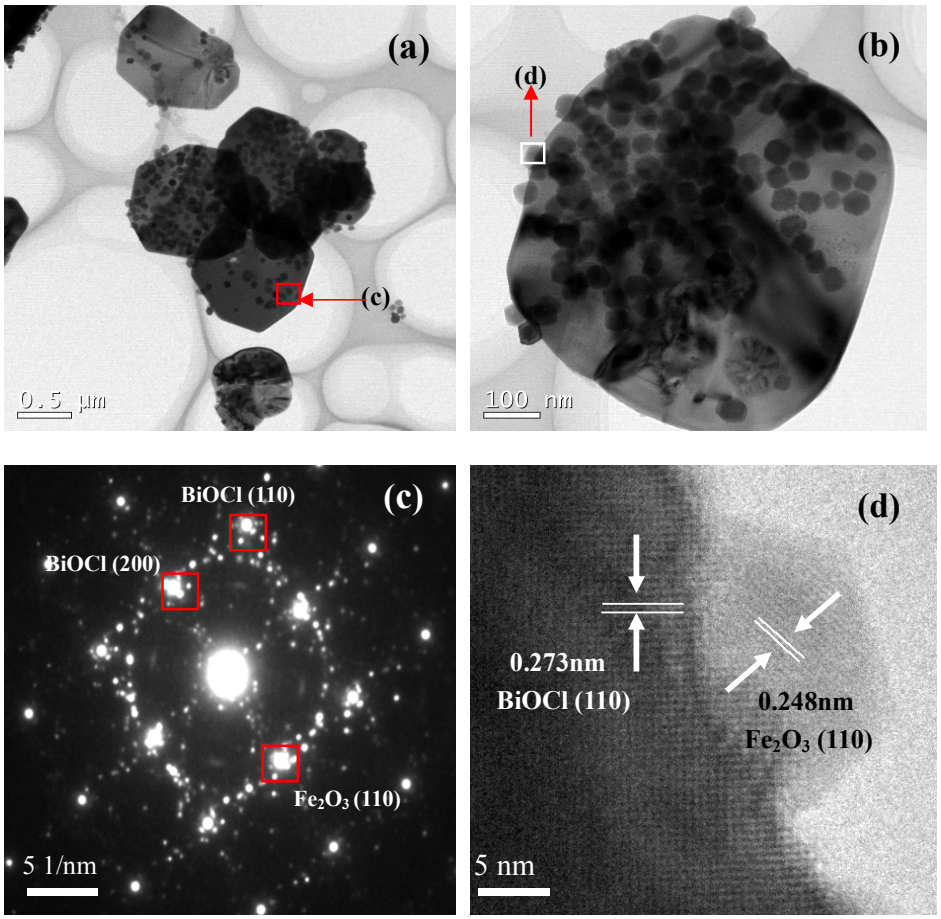

Fig. 5

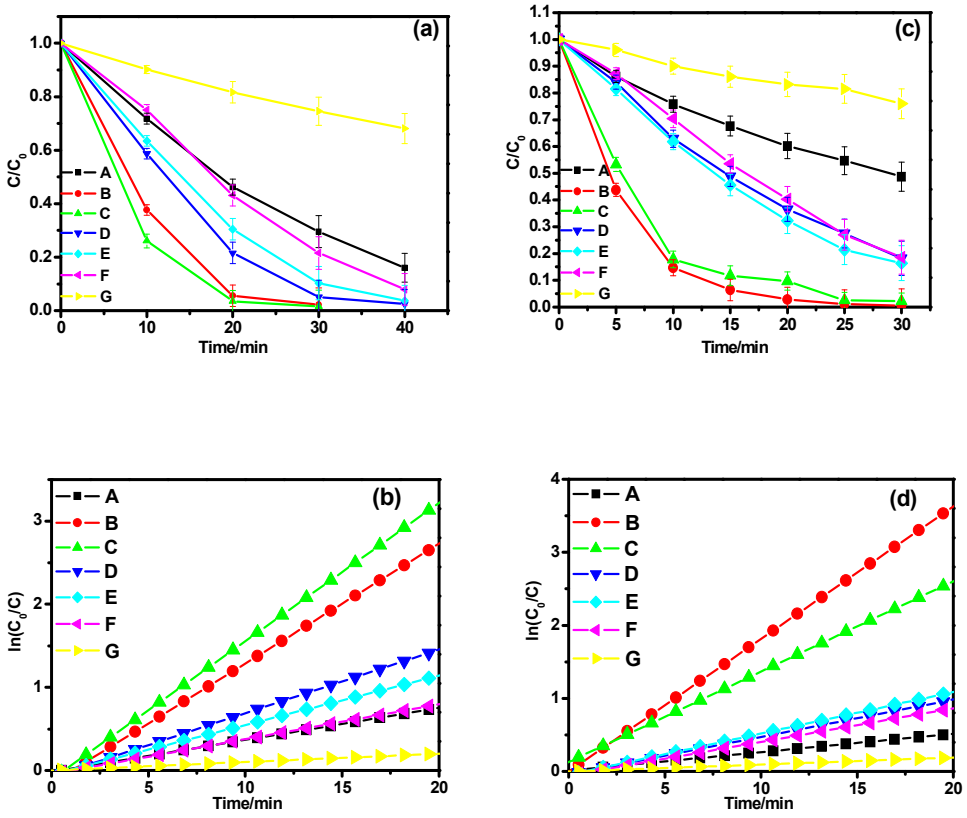

Fig. 6

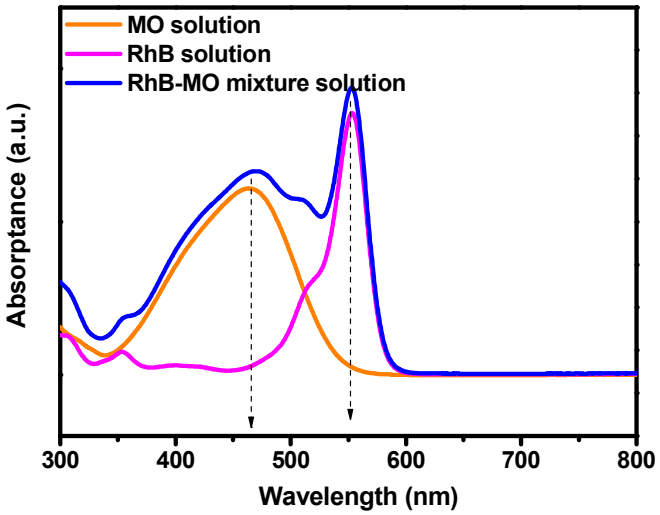

Fig. 7

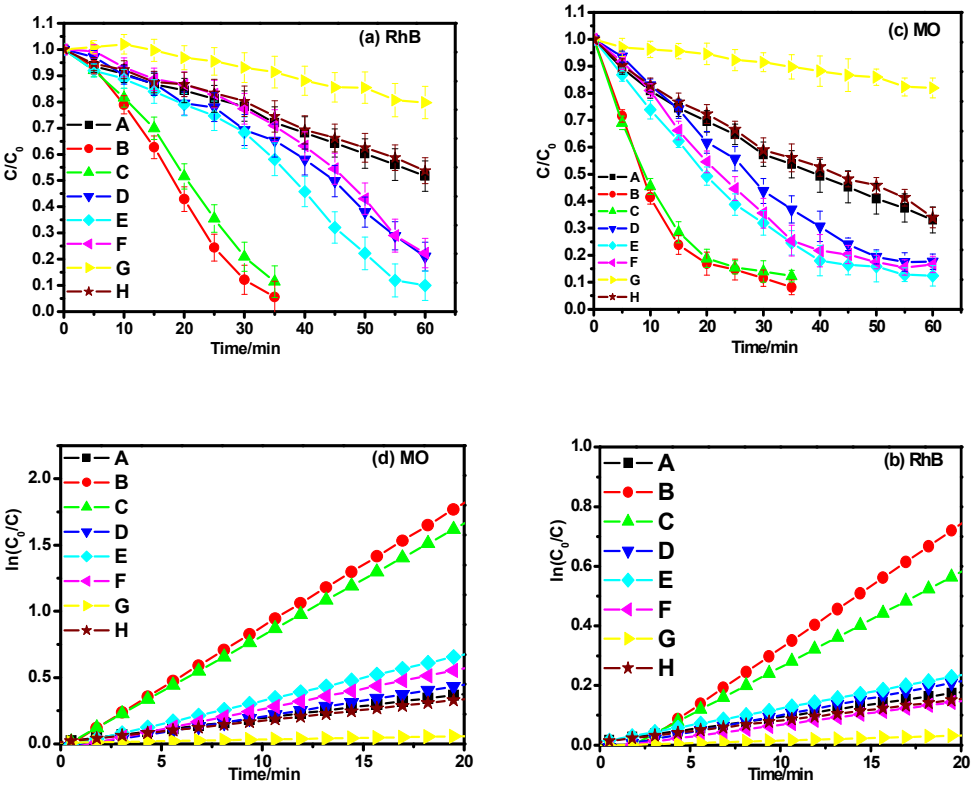

Fig. 8

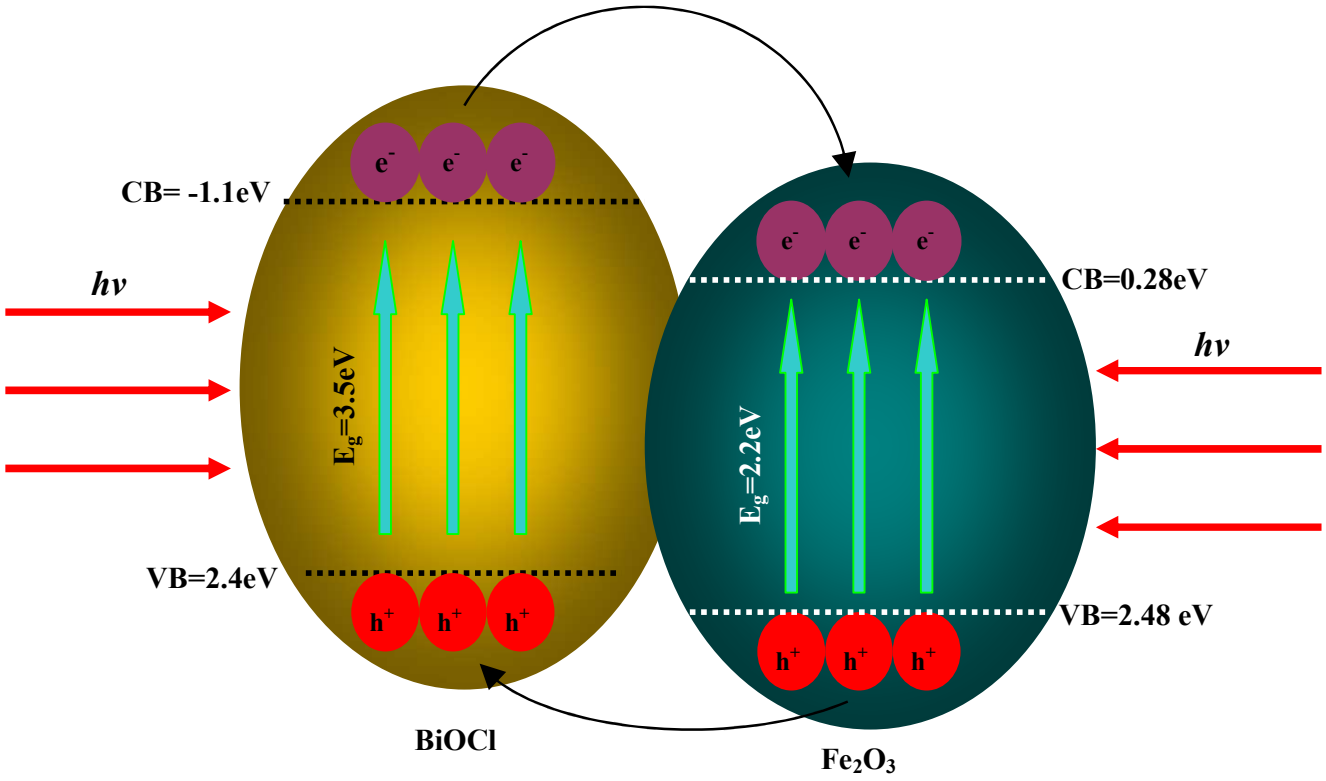

Graphic abstract

Uniform Fe_2O_3/BiOCl p/n heterojunctions are synthesized by an in situ hydrolysis method, whose degradation rates are 4 times higher than that of the bare BiOCl.